Institute of Paper Science and Technology
Atlanta, Georgia

IPST Technical Paper Series Number 906

An Industrial Application of a Mathematical Model of Continuous Flotation Deinking

F. Bloom and S. Shrauti

June 2001

INSTITUTE OF PAPER SCIENCE AND TECHNOLOGY
PURPOSE AND MISSIONS

The Institute of Paper Science and Technology is an independent graduate school, research organization, and information center for science and technology mainly concerned with manufacture and uses of pulp, paper, paperboard, and other forest products and byproducts. Established in 1929 as the Institute of Paper Chemistry, the Institute provides research and information services to the wood, fiber, and allied industries in a unique partnership between education and business. The Institute is supported by 51 member companies. The purpose of the Institute is fulfilled through four missions, which are:

- to provide a multidisciplinary graduate education to students who advance the science and technology of the industry and who rise into leadership positions within the industry;
- to conduct and foster research that creates knowledge to satisfy the technological needs of the industry;
- to provide the information, expertise, and interactive learning that enables customers to improve job knowledge and business performance;
- to aggressively seek out technological opportunities and facilitate the transfer and implementation of those technologies in collaboration with industry partners.

ACCREDITATION

The Institute of Paper Science and Technology is accredited by the Commission on Colleges of the Southern Association of Colleges and Schools to award the Master of Science and Doctor of Philosophy degrees.

NOTICE AND DISCLAIMER

The Institute of Paper Science and Technology (IPST) has provided a high standard of professional service and has put forth its best efforts within the time and funds available for this project. The information and conclusions are advisory and are intended only for internal use by any company who may receive this report. Each company must decide for itself the best approach to solving any problems it may have and how, or whether, this reported information should be considered in its approach.

IPST does not recommend particular products, procedures, materials, or service. These are included only in the interest of completeness within a laboratory context and budgetary constraint. Actual products, materials, and services used may differ and are peculiar to the operations of each company.

In no event shall IPST or its employees and agents have any obligation or liability for damages including, but not limited to, consequential damages arising out of or in connection with any company's use of or inability to use the reported information. IPST provides no warranty or guaranty of results.

An Industrial Application of a Mathematical Model of Continuous Flotation Deinking

by

Frederick Bloom
Department of Mathematical Sciences
Northern Illinois University
DeKalb, IL 60115

and

Suresh Shrauti
Institute of Paper Science and Technology
500 10th St., N.W.
Atlanta, GA 30318

Abstract: A mathematical model is constructed to study the evolution of a continuous flotation process; the model yields a lower bound for the long-time deinking efficiency. The theoretical predictions of the model are analyzed and compared against data obtained, experimentally, at a specific recycle mill.

Keywords: continuous flotation, deinking, kinetic model, rate constant, microprocess probabilities

1 The Continuous Flotation Model

In modelling continuous flotation processes associated with deinking the balance equation for the concentration of free ink particles can be shown to have the form [1]

$$\frac{dn_p^f}{dt} = -k_1 n_p^f + k_2 n_B^a \tag{1.1}$$

In (1.1), k_1 and k_2 are the rate parameters for the forward and reverse reactions respectively; these two parameters depend upon the various microprocess probabilities that comprise the mechanism of bubble/particle aggregate formation and destruction and are functions of the bubble, particle, fluid, and system properties. In [1], the rate parameters, both of which have the dimensions of frequency (i.e. $\sec^{-1}$), were given by

$$k_1 = Z n_B^f P_c P_{asl} P_{tpc} P_{stab} \equiv \bar{k}_1 n_B^f \tag{1.2a}$$

and

$$k_2 = Z' P_{destab} = Z'(1 - P_{stab}) \tag{1.2b}$$

for the case in which it was assumed that only free bubbles may attract a particle; in (1.2a), Zn_B^f plays the role of a collision frequency for the interaction of particles and free bubbles, P_c is the probability of collision between a particle and bubble, P_{asl} is the probability of adhesion by sliding, P_{tpc} is the probability of three-phase contact, P_{stab} is the probability of stability of a bubble/particle aggregate, P_{destab} is the probability of destabilization of a bubble/particle aggregate, and Z' is the detachment frequency (of particles from bubbles). The probability of the formation of a three-phase contact between liquid, bubble, and particle has been shown to be nearly 1 over a wide range of parameters and has been specified to be exactly 1 in this report.

By combining (1.1) with (1.2a) we observe that $Zn_B^f n_p^f$ may be interpreted as the 'collision' rate (per unit volume, per unit time) of free bubbles with free particles, while $P = P_c P_{asl} P_{tpc} P_{stab}$ is the overall probability that a collision will lead to the formation of a

stable bubble/particle aggregate. In an analogous manner, $Z'n_B^a$ may be interpreted as the rate at which bubbles with an attached particle interact (per unit volume, per unit time) with the turbulent vortices in the cell which are responsible for particle detachment, while $P_{destab} = 1 - P_{stab}$ is the probability that such an interaction will actually result in particle detachment. We note that Zn_B^f is time-dependent because of the time-dependence of the quantity n_B^f. In this paper we will replace n_B^f in (1.2a) by n_B^A (the number of bubbles, per unit volume, at time t, which are 'available' to capture particles, $n_B^f \leq n_B^A \leq n_B$); the subsequent replacement of Zn_B^f in (1.2a) by Zn_B^A will still render k_1 time-dependent and for this reason we have denoted k_1, k_2 as 'rate' parameters rather than true 'rate' constants. Only in the most naive model, where all bubbles are available to capture particles, resulting in the replacement, in (1.2a), of Zn_B^f by Zn_B, may k_1 be termed a 'rate' constant.

The probability of stability, P_{stab}, addresses the stabilization/destabilization of a bubble/particle aggregate. Modifying the work of Schulze [2], we take as the form for P_{stab}

$$P_{stab} = 1 - \exp\left[\alpha\left(1 - \frac{1}{Bo'}\right)\right] \tag{1.3}$$

where the modified Bond number (Bo') is defined as the ratio of detachment to attachment forces, i.e.,

$$Bo' = \frac{F_{\text{detachment}}}{F_{\text{attachment}}} = \frac{4R_p^2\left(\Delta\rho_p g + \dfrac{1.9\rho_p\epsilon^{2/3}}{(R_p+R_B)^{1/3}}\right) + 3R_p\left(\dfrac{2\sigma}{R_B} - 2R_B\rho_l g\right)\sin^2\left(\pi - \dfrac{\theta}{2}\right)}{\left|6\sigma\sin\left(\pi - \dfrac{\theta}{2}\right)\sin\left(\pi + \dfrac{\theta}{2}\right)\right|} \tag{1.4}$$

and α, $0 < \alpha \leq 1$, is a stability parameter which depends on the relative particle and bubble radii.

The various other parameters introduced in (1.4) are defined as follows:

$$\begin{cases} R_p & = \text{the particle radius} \\ R_B & = \text{the bubble radius} \\ \epsilon & = \text{the (Kolmogorov) turbulent energy (density (or dissipation rate)} \\ g & = \text{acceleration due to gravity} \\ \sigma & = \text{the surface tension} \\ \theta & = \text{the contact angle} \\ \rho_l & = \text{the fluid density} \\ \rho_p & = \text{the particle density} \\ \Delta\rho_p & = \text{the density difference } (\rho_p - \rho_l) \end{cases} \tag{1.5}$$

In our computations we employ the following relationship among the surface tension, maximum bubble radius, and turbulent energy density (Schulze [3]):

$$\sigma = (2R_{B,\max})^{5/3}\epsilon^{2/3}\rho_l \tag{1.6}$$

For the probabilities of collision (P_c) and adhesion by sliding (P_{asl}) we use, in this paper, new results which were developed, respectively, in Bloom and Heindel [4] and Bloom and Heindel [5] for flotation deinking conditions. Beginning with P_c, if v_p represents particle velocity, and Re_p is the particle Reynolds number

$$Re_p = \frac{2R_p|v_p|}{\nu_l} \tag{1.7}$$

where $\nu_l = \mu_l/\rho_l$ is the kinematic viscosity (μ_l being the usual fluid viscosity), then for an intermediate flow about the bubble surface, in which $2 < Re_p < 500$, it follows from the work in Bloom and Heindel [5] that

$$P_c = \frac{1}{1+|G|}\left[\frac{1}{2(R_p+R_B)^3}\{2R_p^3 + 3R_p^2R_B\} + \frac{2Re_B^*}{(R_p+R_B)^4}\{R_BR_p^3 + 2R_B^2R_p^2\}\right] + \frac{|G|}{1+|G|} \tag{1.8}$$

In (1.8) G is the dimensionless particle settling velocity, i.e.,

$$G = v_{ps}/v_B \tag{1.9}$$

where v_{ps} is the particle settling velocity and v_B is the bubble (terminal) rise velocity. Also,

$$Re_B^* = \frac{1}{15}Re_B^{0.72} \tag{1.10}$$

where Re_B,

$$Re_B = \frac{2v_B R_B}{\nu_l} \tag{1.11}$$

is the bubble Reynolds number. For the same kind of intermediate flow over the bubble surface (e.g., Yoon and Luttrell [6]) it follows from the work of Bloom and Heindel [5] that

$$P_{asl} = \exp\left[-2\left(\frac{\tilde{\lambda}}{C_B}\right)\left(\frac{R_p}{R_B+R_p}\right)\left\{\frac{g(R_B+R_p)-G}{|k(R_B+R_p)|-G}\right\}\left(\frac{h_0}{h_{crit}}-1\right)\right] \tag{1.12}$$

where

$$g(r) = \left(1-\frac{3R_B}{4r}-\frac{R_B^3}{4r^3}\right)+Re_B^*\left(\frac{R_B}{r}+\frac{R_B^3}{r^3}-\frac{2R_B^4}{r^4}\right) \tag{1.13a}$$

and

$$k(r) = -\left\{\left(1-\frac{3R_B}{2r}+\frac{R_B^3}{2r^3}\right)+2Re_B^*\left(\frac{R_B^4}{r^4}-\frac{R_B^3}{r^3}-\frac{R_B^2}{r^2}+\frac{R_B}{r}\right)\right\} \tag{1.13b}$$

while

$$\tilde{\lambda} = 6\pi\mu_l R_p/f \tag{1.14}$$

is the dimensionless friction factor (f the usual fluid flow friction factor). Also, C_B is a measure of the bubble surface mobility and is a parameter which varies between one (for a completely immobilized or rigid bubble surface) and four (for an unrestrained bubble surface), h_0 is the (initial) thickness of the liquid film about the bubble at the instant at which the particle makes contact with the film and begins the sliding process, and $h_{crit} \leq h_0$ is the film thickness at which the film spontaneously ruptures.

In (1.12) it is still necessary to insert the value of $h_o/h_{crit} \equiv \gamma$; actually, because of the manner in which (1.12) is derived, $\gamma = \gamma^* = (h_o/h_{crit})^*$ in (1.12) where the '*' indicates that we using that specific value of h_o/h_{crit} which corresponds to $\phi_o = \phi^* \equiv \phi^*_{crit}$. However, in recent work [7], it has been shown that, for the intermediate flow of Yoon and Luttrell [6], $\gamma^* \simeq 1.5$ and, furthermore, that (1.12) may be replaced by

$$P_{asl} = \left(\frac{3}{2}\right)^{-2\alpha^*} \tag{1.15}$$

where

$$\alpha^* = \frac{1}{C_B}\left(\frac{R_p}{R_B+R_p}\right)\left[\frac{g(R_B+R_p)-G}{\frac{1}{\lambda^*(\phi^*)}|k(R_B+R_p)|-G}\right] \tag{1.16a}$$

$$\lambda^* = \frac{36R_p}{\nu_l Ar}(v_B|k(R_B+R_p)|-v_{ps})\cos\phi^* \tag{1.16b}$$

$$\phi^* = \sin^{-1}\{(3/2)^{-\alpha^*}\} \tag{1.16c}$$

In order to use (1.15), we consider (1.16a,b,c) as a system for (ϕ^*, α^*); we may, either, solve (1.16a,b,c) for ϕ^*, compute α^* using (1.16a,b) and then P_{asl} by employing (1.15) or, by using the computed value of ϕ^*, calculate P_{asl} as $\sin^2\phi^*$. This new algorithm for computing P_{asl} has been used in the work reported here.

Finally it has been shown in [8] that Z, which mediates the collision frequency, and Z', the bubble/particle detachment frequency, may be written in the following forms:

$$\begin{aligned} Z = {} & 5.0(R_p+R_B)^2\sqrt{\bar{U}_p^2+\bar{U}_B^2} \\ & \times\left\{\exp\left[-\frac{1}{2}\frac{(|v_{ps}|+v_B)^2}{\bar{U}_p^2+\bar{U}_B^2}\right]\right\} \\ & +\pi(R_p+R_B)^2\left\{\frac{(|v_{ps}|+v_B)^2+\bar{U}_p^2+\bar{U}_B^2}{|v_{ps}|+v_B}erf\left[\frac{|v_{ps}|+v_B}{\sqrt{2(\bar{U}_p^2+\bar{U}_B^2)}}\right]\right\} \end{aligned} \tag{1.17}$$

with $\mathrm{erf}(x)$ the standard error function and

$$\bar{U}_p = 0.4\frac{\epsilon^{4/9}d_p^{7/9}}{\nu_l^{1/3}}\left(\frac{\rho_p-\rho_l}{\rho_l}\right)^{2/3} \tag{1.18a}$$

$$\bar{U}_B = 0.4\frac{\epsilon^{4/9}d_B^{7/9}}{\nu_l^{1/3}}\left(\frac{|\rho_B-\rho_l|}{\rho_l}\right)^{2/3} \tag{1.18b}$$

the effective values of relative velocity between (respectively) particles (bubbles) and the fluid, while

$$Z' = \sqrt{C_1}\epsilon^{1/3}(d_p+d_B)^{-2/3} \tag{1.19}$$

with C_1 a constant whose value in this report has been taken to be $C_1 = 2$.

As

$$n_p = n_p^f(t) + n_p^a(t) \tag{1.20}$$

with $n_p^a(t)$ denoting the number of particles per unit volume attached to bubbles at time t, and it is assumed that $n_p^a(t) = n_B^a(t)$, we may rewrite (1.1) in the form

$$\frac{dn_p^f}{dt} = -\bar{k}_1 n_p^f n_B + \bar{k}_1 n_p^f (n_p - n_p^f) + k_2(n_p - n_p^f) \tag{1.21}$$

where $\bar{k}_1 = k_1/n_B^f$, i.e.,

$$\bar{k}_1 = ZP_cP_{asl}P_{stab} \tag{1.22}$$

Equation (1.21) must be solved subject to the initial condition that $n_p = n_p^f(0) = n_{po}^f$, where n_{po}^f is the number density of free ink particles at time $t = 0$.

In the balance equation (1.1) for the concentration of free ink particles it was explicitly assumed, by virtue of the presence of the expression n_B^f in the rate parameter (1.2a), that only bubbles which do not already have an ink particle attached to them are capable of picking up a particle and removing it from the flotation cell; we now relax this assumption by replacing n_B^f in (1.2a) by n_B^A where $n_B^A \geq n_B^f$ represents the concentration of bubbles which are available to pick up ink particles. Assuming no bubble/particle aggregate rotation as it rises in the flotation cell, n_B^A represents all bubbles up to (and including) those with one particle less than the maximum number of particles which may be packed, geometrically, on the upper hemisphere of a given bubble. Furthermore, it will be assumed in this report that the expressions for $P_c, P_{asl}, P_{stab}, Z$, and Z' have the explicit forms/values delineated in this section irrespective of the number of particles actually attached to individual bubbles.

Finally, because we no longer assume that the concentration of bubbles with particles attached to them is identical to the concentration of particles attached to bubbles, in the detachment term on the right-hand side of (1.1) we must replace n_B^a by n_p^a. Therefore, in lieu of the balance equation (1.1) we consider the model whose first equation has the form

$$\frac{dn_p^f}{dt} = -k_1 n_p^f + k_2 n_p^a \tag{1.23}$$

where k_2 is still given by (1.2b) but, now,

$$k_1 = Zn_B^A P_c P_{asl} P_{tpc} P_{stab} \equiv \bar{k}_1 n_B^A \tag{1.24}$$

We also let $\Lambda(t)$ represent *the average number of particles, at time t, which are attached to a bubble in the exit stream.* If each bubble with attached particles is carrying only one ink particle then $\Lambda(t) \equiv 1$.

The following relations are obvious and are a direct consequence of the definitions of $n_B, n_B^f, n_B^A, n_p^f, n_p^a$, and n_p, namely

$$n_B^f(t) \leq n_B^A(t) \leq n_B \tag{1.25}$$

and

$$n_B^a \leq n_p^a = n_p - n_p^f \tag{1.26}$$

By virtue of (1.25)

$$-n_B^A(t) \leq -n_B^f(t) \tag{1.27}$$

Using this result in (1.23) we have, in view of (1.24),

$$\begin{aligned} \frac{dn_p^f}{dt} &\leq -\bar{k}_1 n_p^f n_B^f + k_2 n_p^a \\ &= -\bar{k}_1 n_p^f (n_B - n_B^a) + k_2 (n_p - n_p^f) \end{aligned} \tag{1.28}$$

The differential inequality (1.28) is coupled to the initial condition

$$n_p^f(0) = n_{po}^f = n_p \tag{1.29}$$

We will study solutions of the system (1.28), (1.29) with the goal of producing an upper bound for $n_p^f(t)$; an upper bound for $n_p^f(t)$ will, of course, yield a lower bound for the efficiency

$$\text{Eff}(t) = 1 - \gamma(t) \equiv 1 - (n_p^f(t)/n_p) \tag{1.30}$$

By virtue of (1.28) we have

$$\frac{dn_p^f}{dt} \leq -\bar{k}_1 n_p^f n_B + \bar{k}_1 n_p^f n_B^a + k_2 (n_p - n_p^f) \tag{1.31}$$

However, in view of the definition of Λ,

$$n_B^a = \frac{1}{\Lambda} n_p^a$$

and, therefore, (1.31) may be rewritten in the form

$$\frac{dn_p^f}{dt} \leq -\bar{k}_1 n_p^f n_B + \left(\frac{\bar{k}_1}{\Lambda}\right) n_p^f (n_p - n_p^f) + k_2 (n_p - n_p^f) \tag{1.32}$$

A particularly conservative approach, at this junction, would consist, e.g., of taking the maximum carrying capacity of a bubble to be the maximum number (K) of particles that can attach to a typical bubble in the flotation cell along an arc (on one hemisphere) of a great circle on the bubble. We note that K is a function only of the radii R_p and R_B of the particle and bubble, respectively; in fact it is easily shown that $(2\alpha)K \leq \pi$ so that, in fact, we may take

$$K = \left[\frac{\pi}{2\alpha}\right] + 1 \tag{1.33}$$

if $\left[\frac{\pi}{2\alpha}\right]$ is odd and

$$K = \left[\frac{\pi}{2\alpha}\right] \tag{1.34}$$

if $\left[\frac{\pi}{2\alpha}\right]$ is even, where $[z]$ denotes the greater integer less than or equal to z. For $R_p << R_B$ we have

$$\sin\alpha \approx \alpha \approx \frac{R_p}{R_B + R_p} \tag{1.35}$$

so that

$$K = \left[\frac{\pi}{2}\left(1 + \left(\frac{R_B}{R_p}\right)\right)\right] \tag{1.36}$$

Thus, for the concentration of bubbles available to capture particles at any time t we have

$$n_B^A = n_B - n_B^{a,K} \tag{1.37}$$

while for the concentrations, respectively, of bubbles with particles attached to them, and of particles attached to bubbles, we have

$$n_B^a = \sum_{j=1}^{K} n_B^{a,j} \tag{1.38}$$

and

$$n_p^a = \sum_{j=1}^{K} j n_B^{a,j} \tag{1.39}$$

Therefore,

$$n_B = n_B^A + n_B^{a,K} \equiv \sum_{j=0}^{K-1} n_B^{a,j} + n_B^{a,K} = \sum_{j=0}^{K} n_B^{a,j} \tag{1.40}$$

and

$$\Lambda = \frac{n_p^a}{n_B^a} \equiv \left(\sum_{j=1}^{K} j n_B^{a,j} / \sum_{j=1}^{K} n_B^{a,j} \right) \tag{1.41}$$

We note that $\Lambda \geq 1$ and $\Lambda = 1$ if and only if $n_B^{a,j} = 0$ for $j \geq 2$.

In order to more precisely specify the quantity Λ we may assume the existence of an experimentally determined distribution function

$$f(x) = n_B^{a,x} \tag{1.42}$$

to represent the concentration of bubbles which have exactly x particles attached to them. In actuality, of course, the concentration of bubbles which have a fixed number x of particles attached to them will fluctuate with time; in a first model, however, we may assume that for fixed x, $f(x)$ represents an average over a time interval $[0, T]$ of interest in the problem, i.e.,

$$f(x) = \frac{1}{T} \int_0^T n_B^{a,x}(t) dt \equiv \bar{n}_B^{a,x} \tag{1.43}$$

In implementing the model, this assumption is used only to deal with the coefficient involving Λ in (1.32).

In (1.43) x is a nonnegative integer which varies from zero up to the maximum carrying capacity of one hemisphere of a typically sized bubble. In order to illustrate the type of results which are possible with an experimentally determined distribution function $f(x)$, let us assume that $f(x)$ is proportional to a normally distributed random variable with mean $\frac{1}{2}K$, variance $\bar{\sigma}^2$, and standard deviation $\bar{\sigma}$, i.e., with the constant of proportionality denoted by k

$$f(x) = \frac{k}{\sqrt{2\pi}\bar{\sigma}} e^{-(x-\frac{1}{2}K)^2/2\bar{\sigma}^2} \tag{1.44}$$

for $0 \leq x < \infty$, with $f(x) \equiv 0$ for $x < 0$. We may think of $f(x)$, as given by (1.44), as interpolating the values of f at nonnegative integer values x because $\bar{n}_B^{a,x}$ is meaningful, physically, only at such values. The constant of proportionality k in (1.44) can be determined as follows: for $x = K/2$

$$f(K/2) = \bar{n}_B^{a,K/2} = \frac{k}{\sqrt{2\pi}\bar{\sigma}} \tag{1.45}$$

Thus,

$$k = \sqrt{2\pi}\bar{\sigma}\bar{n}_B^{a,K/2} \tag{1.46}$$

so that

$$f(x) = \bar{n}_B^{a,K/2} e^{-(x-\frac{1}{2}K)^2/2\bar{\sigma}^2} \tag{1.47}$$

From (1.47) it follows that

$$f(0) = f(K) = \bar{n}_B^{a,K/2} e^{-K^2/8\bar{\sigma}^2} \tag{1.48}$$

Remarks: We note that

$$\begin{aligned} n_B &= \sum_{j=0}^{K} n_B^{a,j} \\ &= \sum_{j=0}^{K} \bar{n}_B^{a,j} \\ &= \sum_{j=0}^{K} f(j) \\ &= \bar{n}_B^{a,K/2} \sum_{j=0}^{K} e^{-(j-\frac{1}{2}K^2)2\bar{\sigma}^2} \\ &\equiv \bar{n}_B^{a,K/2} F(K;\bar{\sigma}) \end{aligned}$$

Thus,

$$\bar{n}_B^{a,K/2} = n_B / F(K;\bar{\sigma}) \tag{1.49}$$

where

$$F(K;\sigma) = \sum_{j=0}^{K} e^{-(j-K/2)^2/2\bar{\sigma}^2} \tag{1.50}$$

Using (1.49), (1.50), we may rewrite (1.47) in the form

$$f(x) = \frac{n_B}{F(K;\sigma)} e^{-(x-\frac{1}{2}K)^2/2\bar{\sigma}^2}, \; 0 \leq x < \infty \tag{1.51}$$

In (1.32), Λ as given by (1.41) will, in general, fluctuate with time; so as not to have to deal with a system with time-dependent coefficients we now replace Λ in (1.41) by

$$\bar{\Lambda} = \sum_{j=1}^{K} j\bar{n}_B^{a,j} \Big/ \sum_{j=1}^{K} \bar{n}_B^{a,j} \tag{1.52}$$

so that

$$n_p^a = \bar{\Lambda} n_B^a \tag{1.53}$$

in which case (1.32) holds with Λ replaced by $\bar{\Lambda}$. From (1.52), (1.43), and (1.44) it now follows that

$$\begin{aligned} \bar{\Lambda} &= \sum_{j=1}^{K} j f(j) \Big/ \sum_{j=1}^{K} f(j) \\ &= \sum_{j=1}^{K} j e^{-(j-\frac{1}{2}K)^2/2\bar{\sigma}^2} \Big/ \sum_{j=1}^{K} e^{-(j-\frac{1}{2}K)^2/2\bar{\sigma}^2} \\ &\equiv G(K;\bar{\sigma}) \end{aligned} \tag{1.54}$$

The model under consideration is based on the differential inequality (1.32); this inequality is subject to the constraint that n_B and n_p are constant as well as to the initial condition (1.29).

In (1.32)

$$\bar{k}_1 = Z P_c P_{asl} P_{stab} \tag{1.55a}$$

$$k_2 = Z'(1 - P_{stab}) \tag{1.55b}$$

and $\bar{\Lambda}$ is the (time-averaged) average number of particles attached to those bubbles with attached particles; for the Gaussian distribution considered above e.g., $\bar{\Lambda}$ would be given by $G(K;\sigma)$, as defined in (1.54). An upper bound for the set of solutions of (1.32), (1.29) is obtained by considering (1.32) with inequality replaced by equality, i.e.,

$$\frac{dn_p^f}{dt} = -\bar{k}_1 n_p^f n_B + \left(\frac{\bar{k}_1}{\bar{\Lambda}}\right) n_p^f (n_p - n_p^f) + k_2(n_p - n_p^f) \tag{1.56}$$

which we may rewrite in the form

$$\frac{dn_p^f}{dt} = -\left(\frac{\bar{k}_1}{\bar{\Lambda}}\right)(n_p^f)^2 + \left[\bar{k}_1\left(\frac{n_p}{\bar{\Lambda}} - n_B\right) - k_2\right] n_p^f + k_2 n_p \tag{1.57}$$

If we now set

$$\gamma(t) = n_p^f(t)/n_p \tag{1.58}$$

then (1.57) assumes the form

$$\dot{\gamma}(t) = -\left(\frac{\bar{k}_1 n_p}{\bar{\Lambda}}\right)\gamma^2 + \left[\bar{k}_1\left(\frac{n_p}{\bar{\Lambda}} - n_B\right) - k_2\right]\gamma + k_2 \tag{1.59}$$

Finally, we assume that $n_p < \bar{\Lambda} n_B$ and set

$$A = \frac{\bar{k}_1 n_p}{\bar{\Lambda}},\ B = \kappa\bar{k}_1 - k_2,\ C = k_2 \tag{1.60}$$

where

$$\kappa = \frac{n_p}{\bar{\Lambda}} - n_B < 0 \tag{1.61}$$

Employing the definitions in (1.60), (1.61) and replacing $\gamma(t)$ by $\Gamma(t) = -\gamma(t)$ in (1.59) we obtain

$$\dot{\Gamma}(t) = A\Gamma^2(t) + B\Gamma(t) - C \tag{1.62a}$$

with the associated initial condition

$$\Gamma(0) \equiv -\frac{n_p^f(0)}{n_p} = -1 \tag{1.62b}$$

2 Model Solutions

To integrate the model system (1.62a,b) we write (1.62a) in the form

$$\dot{\Gamma}(t) = A\left[\left(\Gamma(t) + \frac{B}{2A}\right)^2 - \left(\frac{B^2}{4A^2} + \frac{C}{A}\right)\right] \tag{2.1}$$

Because

$$\frac{B^2}{4A^2} + \frac{C}{A} > 0$$

there exists a $\mu > 0$ such that

$$\mu^2 = \frac{B^2}{4A^2} + \frac{C}{A} \tag{2.2}$$

Thus, if we set

$$x(t) = \Gamma(t) + \frac{B}{2A} \tag{2.3}$$

then (2.1) becomes, for $t > 0$,

$$\dot{x}(t) = A(x^2(t) - \mu^2) \tag{2.4}$$

and associated with (2.4) is the initial condition

$$x(0) = \frac{B}{2A} - 1 \tag{2.5}$$

If $x^2(t) > \mu^2$, for all $t > 0$, then as $A > 0$ it follows that $\dot{x}(t) > 0$ for all $t > 0$ and this, in turn, is equivalent to $\dot{\gamma}(t) < 0$ for all $t > 0$.

Remarks: In view of the definitions of A and B we have the explicit expressions

$$x(t) = \frac{-n_p^f(t)}{n_p} + \frac{\left(\frac{n_p}{\bar{\Lambda}} - n_B\right)\bar{k}_1 - k_2}{2\bar{k}_1 n_p/\bar{\Lambda}}$$

or

$$x(t) = \frac{-n_p^f(t)}{n_p} + \frac{(n_p - \bar{\Lambda}n_B)\bar{k}_1 - k_2\bar{\Lambda}}{2\bar{k}_1 n_p} \tag{2.6}$$

and

$$\mu = \sqrt{\frac{[(n_p - \bar{\Lambda}n_B)\bar{k}_1 - k_2\bar{\Lambda}]^2}{4\bar{k}_1^2 n_p^2} + \frac{k_2\bar{\Lambda}}{\bar{k}_1 n_p}} \tag{2.7}$$

while

$$x(0) = \frac{(n_p - \bar{\Lambda}n_B)\bar{k}_1 - k_2\bar{\Lambda}}{2\bar{k}_1 n_p} - 1 \tag{2.8}$$

By virtue of (1.61), $x(0) < 0$.

Returning to the model system written in terms of $x(t)$, we note that (2.4) is a separable, first-order equation which may be integrated explicitly so as to yield

$$\frac{1}{2\mu}\left\{ln\left[\frac{x(t)-\mu}{x(t)+\mu}\right] - ln\left[\frac{x(0)-\mu}{x(0)+\mu}\right]\right\} = At \tag{2.9}$$

for $t > 0$. Equation (2.9) has been obtained under the hypothesis that $x^2(t) > \mu^2$, for all $t \geq 0$; this hypothesis will be substantiated below. If we now set

$$\beta_0 = \frac{x(0)-\mu}{x(0)+\mu} \tag{2.10}$$

then it follows from (2.9) that

$$x(t) = \mu \frac{1 + \beta_0 e^{2\mu A t}}{1 - \beta_0 e^{2\mu A t}}, \; t \geq 0 \tag{2.11}$$

As $x(0) < 0$, $x(0) - \mu < 0$, where μ is given explicitly by (2.7). In order, therefore, to conclude that β_0 as defined by (2.10) satisfies $\beta_0 > 0$ we need a conditions which implies that $x(0) + \mu < 0$. However,

$$x(0) + \mu = -1 + \frac{B}{2A} + \mu \tag{2.12}$$

while

$$\mu = \sqrt{\frac{B^2}{4A^2} + \frac{C}{A}} > \frac{|B|}{2A} \tag{2.13}$$

Thus

$$x(0) + \mu > -1 + \frac{B}{2A} + \frac{|B|}{2A} = -1 \tag{2.14}$$

as $B < 0$. On the other hand

$$\mu < \frac{|B|}{2A} + \sqrt{\frac{C}{A}} \tag{2.15}$$

so that

$$x(0) + \mu < -1 + \sqrt{\frac{C}{A}} \tag{2.16}$$

Combining (2.14) and (2.16) we obtain

$$-1 < x(0) + \mu < -1 + \sqrt{\frac{C}{A}} \tag{2.17}$$

Therefore, $x(0) + \mu < 0$ provided $C < A$, i.e., provided

$$k_2 < \frac{\bar{k}_1 n_p}{\bar{\Lambda}} \tag{2.18}$$

As $x(0) < 0$, $x(0) = -|x(0)|$, and (2.10) may be written in the form

$$\beta_0 = \frac{|x(0)| + \mu}{|x(0)| - \mu} \tag{2.19}$$

But, we have shown that (2.18) implies that $\beta_0 > 0$ and, as $\mu > 0$, it then follows from (2.19) that $|x(0)| > \mu$ in which case $\beta_0 > 1$. From (2.11) we obtain

$$\dot{x}(t) = \frac{4\mu^2 \beta_0 e^{2\mu A t}}{(1 - \beta_0 e^{2\mu A t})^2} \tag{2.20}$$

But $\beta_0 > 1$, so $1 - \beta_0 e^{2\mu At} \neq 0$, $\forall t \geq 0$, and it then follows from (2.20) that $\dot{x}(t) > 0$, for all $t > 0$. A direct computation shows that $x(t)$, as defined by (2.11), satisfies both (2.4) and (2.5) and, therefore, by local uniqueness of the solution of the initial-value problem we conclude that (2.11) is the unique solution of (2.4), (2.5). Thus, $x(t)$, as given by (2.11) satisfies

$$\frac{\dot{x}(t)}{A} = x^2(t) - \mu^2, \; t > 0$$

But $\dot{x}(t) > 0, t > 0$, and $A > 0$ so $x(t)$, as given by (2.11) also satisfies $x^2(t) > \mu^2$, for all $t > 0$.

3 Theoretical Model Predictions

We write the solution (2.11) to the initial-value problem (2.4), (2.5) in the form

$$\gamma(t) = \mu \left[\frac{\beta_0 e^{2\mu At} + 1}{\beta_0 e^{2\mu At} - 1} \right] + \frac{B}{2A}$$

or, as $B < 0$,

$$\gamma(t) = \mu \left[\frac{1 + (1/\beta_0) e^{-2\mu At}}{1 - (1/\beta_0) e^{-2\mu At}} \right] - \frac{|B|}{2A} \tag{3.1}$$

It follows at once from (3.1) that

$$\lim_{t \to \infty} \gamma(t) = \mu - \frac{|B|}{2A} \tag{3.2}$$

or, in view of (1.60), (1.61), (2.7), and the definition of γ

$$\lim_{t \to \infty} \frac{n_p^f(t)}{n_p} = \sqrt{\frac{[(n_p - \bar{\Lambda} n_B)\bar{k}_1 - k_2 \bar{\Lambda}]^2}{4\bar{k}_1^2 n_p^2} + \frac{k_2 \bar{\Lambda}}{\bar{k}_1 n_p}} - \frac{[(n_p - \bar{\Lambda} n_B)\bar{k}_1 - k_2 \bar{\Lambda}]}{2\bar{k}_1 n_p} \tag{3.3}$$

Furthermore, for

$$\frac{C}{A} = \frac{\bar{\Lambda} k_2}{n_p \bar{k}_1}$$

small (the expected situation) the mean-value theorem may be used to approximate the right-hand side of (3.2) as follows:

$$\begin{aligned}\mu - \frac{|B|}{2A} &= \sqrt{\frac{B^2}{4A^2} + \frac{C}{A}} - \frac{|B|}{2A} \\ &\simeq \left(\frac{1}{2\sqrt{\lambda}}\Big|_{\lambda=(B^2/4A^2)}\right)\left(\frac{C}{A}\right) \\ &= \frac{C}{|B|}\end{aligned}$$

in which case (3.2) yields

$$\lim_{t\to\infty} \frac{n_p^f(t)}{n_p} = \frac{k_2}{\left(n_B - \frac{n_p}{\bar{\Lambda}}\right)\bar{k}_1 + k_2} \equiv \gamma_\infty \tag{3.4}$$

Alternatively, we may write for the large time asymptotic limit of the number of free particles

$$\lim_{t\to\infty} n_p^f(t) = \frac{k_2 n_p}{\left(n_B - \frac{n_p}{\bar{\Lambda}}\right)\bar{k}_1 + k_2} \equiv n_{p,\infty}^f \tag{3.5}$$

From (2.3) and the fact that $\Gamma(t) = -\gamma(t)$ we obtain $\dot{x}(t) = -\dot{\gamma}(t)$ in which case (2.20) produces

$$\dot{\gamma}(t) = \frac{-4\mu^2 A\beta_0 e^{2\mu At}}{(\beta_0 e^{2\mu At} - 1)^2} \tag{3.6}$$

for all $t > 0$. From (3.6) we infer that the graph of $\gamma(t) = n_p^f(t)/n_p$ is (strictly) monotonically decreasing for all $t > 0$. Furthermore,

$$\ddot{\gamma} = 8\mu^3 A^2 \beta_0 e^{2\mu At}\left[\frac{\beta_0 e^{2\mu At} + 1}{(\beta_0 e^{2\mu At} - 1)^3}\right] > 0 \tag{3.7}$$

for all $t > 0$, so that the graph of $\gamma(t)$ is convex for all $t > 0$. The initial slope $\dot{\gamma}(0)$ of the graph of $\gamma(t)$ is given by

$$\dot{\gamma}(0) = \frac{-4\mu^2 A\beta_0}{(\beta_0 - 1)^2} < 0 \tag{3.8}$$

and, thus, the equation of the tangent line to the graph of $\gamma(t)$ at time $t = 0$ is

$$\bar{\gamma}(t) = \frac{-4\mu^2 A\beta_0}{(\beta_0 - 1)^2} t + 1 \tag{3.9}$$

From (3.9) we easily obtain the value of that time $\bar{t}$ at which the tangent line $\bar{\gamma}(t)$ to $\gamma(t)$, at $t = 0$, intersects the asymptotic level $\gamma = \gamma_\infty$ (as given by (3.4)):

$$\bar{t} = \frac{1 - \gamma_\infty}{4\mu^2 A \beta_0}(\beta_0 - 1)^2 \tag{3.10}$$

The larger the initial rate of decline of free particles the smaller the value of $\bar{t}$.

Now let t^* represent the time required for $\gamma(t)$, the ratio of free ink particles to the (constant) total number of ink particles, to fall to a specified level γ^*, $\gamma_\infty < \gamma^* < 1$. Then from (3.1) we easily compute that

$$t^* = \frac{1}{2\mu A} ln \left[\frac{1}{\beta_0} \left\{ \frac{\frac{1}{\mu}\left(\gamma^* + \frac{|B|}{2A}\right) + 1}{\frac{1}{\mu}\left(\gamma^* + \frac{|B|}{2A}\right) - 1} \right\} \right] \tag{3.11}$$

In particular if $\gamma^* = \frac{1}{2}$ then $t^* = t_{1/2}$, the time required for the ratio of free ink particles to the (constant) total number of ink particles to fall to $\frac{1}{2}$; by virtue of (3.11) this ratio is given by

$$t_{1/2} = \frac{1}{2\mu A} ln \left[\frac{1}{\beta_0} \left\{ \frac{\frac{1}{\mu}\left(\frac{1 + |B|/A}{2}\right) + 1}{\frac{1}{\mu}\left(\frac{1 + |B|/A}{2}\right) - 1} \right\} \right] \tag{3.12}$$

A useful approximation to $t_{1/2}$ may be obtained by working with the tangent line to the graph of $\gamma(t)$ at $t = 0$, i.e., with $\bar{\gamma}(t)$ as given by (3.9); we let $\bar{t}_{1/2}$ represent the time at which this tangent line intersects the level $\gamma = \frac{1}{2}$, i.e.,

$$\bar{t}_{1/2} = \frac{1}{8} \cdot \frac{(\beta_0 - 1)^2}{\mu^2 A \beta_0} \tag{3.13}$$

Now,

$$\beta_0 = \frac{|x(0)| + \mu}{|x(0)| - \mu}$$

so

$$\beta_0 - 1 = \frac{|x(0)| + \mu}{|x(0)| - \mu} - 1 = \frac{2\mu}{|x(0)| - \mu}$$

and, thus, (3.13) may be reduced to

$$\bar{t}_{1/2} = \frac{1}{2A} \cdot \frac{1}{|x(0)|^2 - \mu^2} \tag{3.14}$$

Using (2.7) and (2.8) we easily obtain

$$\begin{aligned} |x(0)|^2 - \mu^2 &= 1 - \left\{ \frac{(n_p - \bar{\Lambda} n_B)}{n_p} \right\} \\ &\equiv \bar{\Lambda} \left(\frac{n_B}{n_p} \right) \end{aligned} \tag{3.15}$$

Thus, from (3.14), (3.15), and (1.60)

$$\bar{t}_{1/2} = 1/2\bar{k}_1 n_B \tag{3.16}$$

Also, the magnitude of the initial rate of decrease of free particles is, by virtue of (3.8),

$$\begin{aligned} |\dot{\gamma}(0)| &= 4\mu^2 A\beta_0/(\beta_0 - 1)^2 \\ &= A(|x(0)|^2 - \mu^2) \\ &= \bar{k}_1 n_B \end{aligned} \tag{3.17}$$

Because both (3.16) and (3.17) are based on the tangent line approximation to the graph of $\gamma(t)$ at $t = 0$, neither result involves the kinetic constant k_2 which mediates detachment of particles from bubbles. A measure of the efficiency of the deinking process which involves both $\bar{k}_1$ and k_2 is, of course, $t_{1/2}$ which may be written in the form

$$t_{1/2} = \frac{1}{2\mu A} \left\{ ln \left[\frac{(A + |B| + 2\mu A)}{(A + |B| - 2\mu A)} \right] - ln\beta_0 \right\} \tag{3.18}$$

A second measure of the efficiency of the deinking process which we have is represented by the large time limit of the ratio $n_p^f(t)/n_p$ as given by either (3.3) or by the approximate expression (3.4); this measure also exhibits the competition between attachment and detachment of particles to/from bubbles and may be written as

$$\gamma_\infty = \frac{1}{\left(n_B - \frac{n_p}{\bar{\Lambda}} \right) \frac{\bar{k}_1}{k_2} + 1} \tag{3.19}$$

if we work with the approximation in (3.4). Clearly, for fixed n_p, n_B, and $\bar{\Lambda}$, as $\bar{k}_1 \uparrow$, $\gamma_\infty \downarrow$ and as $k_2 \downarrow$, $\gamma_\infty \downarrow$. A lower bound for the actual efficiency of the deinking process, as gauged by the model, is given by (1.30) and (3.1), i.e.,

$$Eff(t) = 1 + \frac{|B|}{2A} - \mu \left[\frac{1 + \beta_0^{-1} e^{-2\mu A t}}{1 - \beta_0^{-1} e^{-2\mu A t}} \right] \tag{3.20}$$

while a lower bound for the asymptotic (large-time) efficiency is determined, by virtue of (3.19) as

$$\begin{aligned} Eff(\infty) &\geq 1 + \frac{|B|}{2A} - \mu \\ &\simeq 1 - \left[1 / \left\{ \left(n_B - \frac{n_p}{\bar{\Lambda}} \right) \frac{\bar{k}_1}{k_2} + 1 \right\} \right] \end{aligned} \tag{3.21}$$

Remarks: By using the definitions of $\bar{k}_1$ and k_2 it is an easy algebraic exercise to rewrite the lower-bound (3.21) for the asymptotic efficiency $Eff(\infty)$ in the form

$$Eff(\infty) = 1 - \frac{1}{KM \left(\frac{P_{stab}}{1 - P_{stab}} \right) + 1} \tag{3.22}$$

where

$$\begin{cases} K = n_B - \dfrac{n_p}{\Lambda} \\ M = \left(\dfrac{Z}{Z'} \right) P_c P_{asl} \end{cases} \tag{3.23}$$

Insertion of the expression (1.3), for P_{stab}, into (3.22) then yields as a lower-bound

$$Eff(\infty) = \frac{1}{KM(e^{\alpha P} - 1) + 1} \tag{3.24}$$

where

$$P = \frac{1}{Bo' - 1} \tag{3.25}$$

Bo' is the modified bond number, as given by (1.4), and α, $0 < \alpha \leq 1$, is the stability parameter associated with particle/bubble aggregate stability. The relation (3.24) thus displays the functional dependence of the asymptotic efficiency $Eff(\infty)$ on the parameter α.

4 Experimental Methodology

Flotation deinking trials were performed on the B-line at Abitibi's recycle mill in Sheldon, Texas. The B-line consists of a mixing cell, 7 primary Ecocells and two secondary cells manufactured by Voith Sulzer. Only two variables, feed flow rate and feed consistency, were varied for the initial experiments. Table 1 shows the experimental conditions that were varied for the five experiments that were conducted. A total of seventeen samples were collected from experiment 1. Twelve samples were collected from each of the remaining four experiments. The samples were shipped immediately and stored in a cold room upon arrival. The samples were then tested for consistency, made into handsheets, and used for ERIC analysis and dirt count measurements. The ERIC and dirt count measurements were performed at the laboratories of Eka Chemicals in Marietta, Georgia.

(a) Surface Tension Measurement

Aliquots of the 64 mill samples were filtered through a Whatman No. 4 filter paper and the filtrates were used to determine the surface tension. Approximately 100 ml of the filtrates was collected from each sample. Surface tension was measured using a Cahn DCA 312 apparatus (Wilhelmy plate method). Tables 2-6 list the data for the surface tension measurements. It is observed that the surface tension of the overflows is lower than that of the other samples for all the experiments. In general, the range of surface tension values lies between 41-44 dynes/cm for all overflows and primary rejects, and between 45-50 dynes/cm for all other samples.

(b) Handsheet making procedure

First, the consistency of the pulp samples was determined. The amount of pulp necessary for making a 3 gram handsheet was calculated. The desired amount of pulp was transferred to a graduated cylinder and diluted to 1000 ml using deionized water. A

150-mm filter paper was placed in a leveled, fritted glass Buchner funnel and wetted with deionized water from a wash bottle. Suction was applied to seat the filter paper. With no suction applied to the funnel the 1000 ml stock was rapidly poured. Subsequently, suction was applied until all the excess water was removed. The Buchner funnel was inverted over a standard blotter paper and the test sheet and filter paper were dislodged from the funnel by blowing into the funnel stem. The blotter paper, test sheet and filter paper were placed on a flat surface, covered with an additional blotter paper and couch plate. A couch roll was rolled five times with no pressure being applied except for the weight of the roll, then the couch plate and top blotter were removed, and an indelible pencil was used to identify the test sheet. Next, a sheet of blotter paper was placed on the press. On this blotter was placed a clean drying plate with its polished surface facing upwards. The test sheet with the filter paper was placed face down on the drying plate. Two more blotter papers were then placed on top. The stack (from the bottom) then consisted of one blotter, a drying plate, the test sheet, filter paper, and the two blotters. On this stack a clean drying plate for the next test sheet was added. This sequence was continued till 8 test sheets were accumulated. Care was taken to center the drying sheets. The cover was placed over the final stack and tightened. The pressure was raised to 50 psig in 30 seconds and then maintained for an additional 90 seconds. After removing the press cover, the filter paper was removed from the test sheets. The handsheets were dried using a commercial drum dryer and were then left in a TAPPI humidity and temperature controlled environment until analysis.

(c) Measurement of handsheet properties

An ERIC value is a measure of the ink attachment to the fibers. ERIC values represent an estimate of the amount of ink below 10 micrometers that is in the fiber. Two handsheets were made for each pulp sample that was obtained from the mill. For the measurement of ERIC, three measurements were made on the top side of each handsheet

and three measurements were made on the bottom side of each handsheet. The results were tabulated as the average of the six readings for each side. The ERIC measurements in table 7 were performed on a Technidyne Color Touch ISO instrument. The Ink Scan evaluates the ink particle distribution from 10 micrometers to 200 micrometers. Five measurements were made from the top side of each handsheet and 5 measurements from the bottom side of each sheet for a total of 20 measurements per pulp sample. The average of the twenty measurements is reported in table 8. The particles were divided into three size ranges and the overall efficiency for the flotation line was calculated for the three individual size ranges.

(d) Determination of Model Parameter Values

The data obtained from the five experiments conducted at the recycle mill were compared to the modified model for continuous flotation; as a first step the parameters used in the model had to be identified. The modified model requires thirteen parameters to evaluate the long-time deinking efficiency $Eff(\infty)$. Many of these parameters were measured and some that could not be measured were input as "educated guesses."

Density of fluid and *viscosity* of the pulp in the model were specified to correspond to those of water. The viscosity of fiber suspensions is known to be highly non-Newtonian and will deviate significantly from that of water. Also, the consistency of the fiber suspension will affect the apparent viscosity of the suspension. The effect of viscosity will be further discussed in the section on model parametric variations.

The *particle diameter* was fixed at the upper value in the data range. Since, a significant portion of the ink particles were determined to be in the 8-20 μm size range, the radius of the particles was fixed at 10 μm. The *particle density* was specified to be 1.2g/cm^3.

The *particle concentration* was calculated from the dirt count measurements and the consistency of the feed suspension. Because, a narrow range of 45-50 dynes/cm was

measured for most of the samples in all five experiments, the *surface tension* parameter was assumed to be a constant with a value of 50 dynes/cm. *Contact angle*, a tough parameter to measure, was set at 60°. The *bubble surface mobility* (C_B), was set to a constant value of 1 signifying that the bubbles behaved as rigid spheres.

Power input was computed to be approximately 7.18 W/kg/cell for a recycle line processing 300 tpd (tons per day) at 1.3% consistency (Personal communications with Martin Kemper of Voith Sulzer); this calculation is presented below. It was assumed that the entire power consumed by the line was converted into *turbulent mixing energy*. The calculation proceeds as follows: The inlet pressure of an Ecocell is 0.9 bar. The specific power consumption of a standard Ecocell line is about 27 kWh/ton. A standard Ecocell line consists of 5 primary cells and 1 secondary cell. About 12.5 ton/h are processed. Thus

$$\frac{27kWh}{\text{ton}} \times \frac{12.5 \text{ ton}}{h} = 337kW$$

is the power consumption for a line producing 300 tpd, which is the production rate on line B at Houston. For 5 primary and 1 secondary cell we have a total volume of 46917 L (again, the Houston Mill data). As we assume a density for the slurry of $\rho_{\text{slurry}} = 1\text{g/cm}^3$, 46917 L = 46917 kg slurry. Thus

$$\epsilon = \frac{337,000W}{46917 \text{ kg}} = 7.18 \text{ W/kg}$$

Gas hold-up was not measured and was estimated to be 10%.

Bubble diameter, is a parameter that is currently guessed, and needs to be measured in a mill setting; this parameter appears in each of the equations that determine the probability of the individual microprocesses. Flash X-ray Radiography is not suitable for measuring bubble diameter in a mill environment and an alternate technique has to be utilized. An optical method described by O'Connor et.al. [9] and Hunold et.al. [10] is a good candidate for initial investigation. Using the relationship (1.6) an $R_{B,max}$ of 1.1194

mm may be computed as follows: As 1 W/kg = 10^4 cm^2/sec^3, ϵ = 7.18 W/kg = 7.18 $\times$ 10^4 cm^2/sec^3. For ρ_ℓ we take ρ_ℓ = 1 g/cm^3 while σ is estimated at 50 dynes/cm. Since 1 dyne = 1 g - cm/sec^2 we have σ = 50 g/sec^2. Solving (1.6) for $R_{B,max}$ we find

$$\begin{aligned} R_{b,max} &= \frac{1}{2}\sigma^{\frac{3}{5}}\rho_\ell^{\frac{-3}{5}}\epsilon^{\frac{-2}{5}} \\ &= \frac{1}{2}(50 \text{ g/sec}^2)^{\frac{3}{5}}(1 \text{ g/cm}^3)^{\frac{-3}{5}}(7.18 \times 10^4 \text{ cm}^2/\text{sec}^3)^{\frac{-2}{5}} \\ &= .1194 \text{ cm (or } 1.1194 \text{ mm)} \end{aligned}$$

As $R_{B,\max}$ = 1.1194 mm, a value for R_B of 0.75 mm was selected for use in the model. With R_B and ϵ known, the constant *bubble concentration* can be calculated.

The two remaining parameter are $\overline{\Lambda}$ and α. $\overline{\Lambda}$ represents the average number of ink particles attached to a bubble that has ink particles attached to it. There is no known method of determining this parameter in a mill. For model validation purposes, the value of $\overline{\Lambda}$ was set equal to its minimum value of 1; a parametric variation of $\overline{\Lambda}$ was conducted while maintaining all other parameters constant. The stability parameter α was treated as a fitting parameter. It maybe shown that the model is very sensitive to the value of α. In future work, the parameter α will either be modeled directly or will be backed out (curve fitted) from a set of experimental data.

5 Mill Results vs. Model Predictions

Experimental flotation efficiencies (of ink particles in the 8-20 μm range) for the five experiments at the mill varied between 85 and 90 percent; the upper limit of the size range was used as the particle diameter in the model. Data from experiment 1, wherein standard operating conditions were maintained, was used to determine the value of the fitting parameter α. Maintaining α fixed, the predicted efficiencies of the other experiments were computed. Similar comparisons were made for the deinking efficiency of particles in the 24-52 μm range. Bubble radius was set at 0.75 mm for all the comparisons. Table 9 lists the values of the parameters that were used in the parametric study. In the figures and discussion that follow

it is assumed that all parameters, except the one being varied, are fixed at the values given in table 9. Table 10 lists the comparison of the experimental data with the long time deinking efficiency predicted by the mathematical model.

Figure 1 shows the effect of parameter α on the long time deinking efficiency. It is interesting to note that there are two ranges within which the efficiency is independent of α. The lower range between $0.2 < \alpha < 0.5$ predicts 100% efficiency for the removal of particles with a radius of 10 μm. The $0.6 < \alpha < 1$ range predicts an efficiency of 34% for the same particles. In figure 2 we see the effect of the parameter α on the flotation of ink particles with a radius of 25 μm by bubbles with a radius of 0.75 mm. Here efficiency increases with increasing α values and attains 99 percent at an α value of 0.3.

Variations in the turbulent energy density (ϵ) influence the predicted removal efficiency through the collision rates and the probability of stability. Figure 3 shows the dependence of efficiency on ϵ for α values of both 0.2 and 0.7.

Bubble radius has a variable influence on the long time efficiency. For the value of $\alpha = 0.2$ in figure 4 a bubble larger than 0.90 mm in radius has a negligible effect on the removal efficiency for particles with an R_p of 10 μm.

Figure 5 shows the effect of R_p on the long time efficiency. A high efficiency is predicted by an α of 0.2 at R_p of 10 μm, but efficiency drops significantly for higher values of R_p. For an α value of 0.7 the efficiency rises sharply for particles larger than 10 μm and decreases slightly for particles larger than 75 μm.

Experimentally, feed consistency and feed flow rate were the two factors that were varied during the mill trials. Both of these parameters are not directly required for testing the model. Consistency should be related to the viscosity parameter in the model but a preliminary search of the literature did not provide a mathematical relationship relating viscosity to consistency; such a relationship, between consistency and viscosity, could be obtained (and curve-fitted) from an experimental program. A parametric study of viscosity, holding all

the other parameters at the values given in table 10 is shown in figure 6. The experimental efficiency is shown as the filled circle. The predicted long time efficiency decreases almost linearly with increasing viscosity.

It is widely accepted that there is bubble coalescence at higher consistencies. The effect of bubble coalescence might dominate over the increase in viscosity. Figure 7 shows the change in efficiency due to increase in bubble radius. Experimental efficiency is, once again denoted by the filled circle. For a fixed particle radius, an increase in bubble radius leads to an asymptotic increase in efficiency.

The two main conclusions which follow from the work presented here are the following:

i. The continuous flotation model shows great promise for being able to predict industrial recycle mill efficiencies *if the remaining 'gaps' in the model can be closed, specifically, the measurement of bubble size, the functional form of the stability parameter α, and the relationship between consistency and viscosity.*

ii. Once these 'gaps' in the model are closed the model can also be used to *optimize* mill performance, i.e., it can be used to predict, e.g., the optimal bubble size to use for particles sizes (in a specific range) so as to maximize large-time efficiency. *The model may also be used to determine efficiency at conditions beyond the regime of current equipment.*

References

1. Bloom, F. and T.J. Heindel, "Mathematical Modeling of the Flotation Deinking Process," *Math. Comput. Modelling,* 25, (1997) 13-58.

2. Schulze, H.J., "Flotation as a Heterocoagulation Process: Possibilities of Calculating the Probability of Flotation," in Coagulation and Flocculation, edited by B. Dobias, (1993), 321-353.

3. Schulze, H.J., "Hydrodynamik der Flotations - Elementarvorgänge," Wochenblatt für Papierfabrikation, 122, (1994), 160-168.

4. Bloom, F. and T.J. Heindel, "New Exact and Appropriate Expressions for the Microprocess Probability of Collision in Flotation," J. Colloid and Interface Sci., 213, (1999), 101-111.

5. Bloom, F. and T.J. Heindel, "An Approximate Analytical Expression for the Probability of Attachment by Sliding," J. Colloid and Interface Sci., 218, (1999), 464-577.

6. Yoon, R.H. and G.H. Luttrell, "The Effect of Bubble Size on Fine Particle Flotation," *Mineral Processing and Extractive Metallurgy Review,* 5, (1989), 101-122.

7. Bloom, F., "Modelling the Probability of Adhesion by Sliding", J. Colloid Interface Sci., submitted.

8. Bloom, F. and T.J. Heindel, "On the Structure of Collision and Detachment Frequencies in Flotation Models", Chem Eng. Sci., submitted.

9. O'Connor, C.T., E.W. Randall and C.M. Goodall, "Measurement of the Effects of Physical and Chemical Variables on Bubble Size," International Journal of Mineral Processing, vol 28, pp. 139-149, 1990.

10. Hunold, M., T. Krauthauf, J. Muller, and H.J. Putz, "Effect of Air Volume and Air Bubble Size Distribution of Flotation in Injector-Aerated Deinking Cells," Journal of Pulp and Paper Science, vol. 23, pp. 555-560, 1997.

Nomenclature List

Bo' - modified Bond number

C - $\left(\frac{\bar{k}_1 n_{po}^2}{\bar{\Lambda}}\right) \frac{|r_b|(2\lambda - |r_a|)}{\lambda(|r_b| - |r_a|)}$

C_B - parameter characterizing the bubble surface mobility

C_1 - gas constant

$\mathrm{Eff}(t)$ - global process efficiency at time t : $1 - (n_p^f(t) \big/ n_p)$

$\mathrm{Eff}(t)_1$ - global process efficiency at time t based on the first iteration of $n_p^f(t)$, i.e., on $(n_p^f(t))_1$.

G - dimensionless particle settling velocity

K - maximum number of particles that can attach to a bubble along an arc, on one hemisphere, of a great circle on the bubble

P - $P_c P_{asl} P_{tpc} P_{stab}$, i.e., the overall probability of the formation of a stable bubble/particle aggregate

P_c - probability of collision between a particle and a bubble

P_{asl} - probability of adhesion by sliding

P_{destab} - probability of destabilization of a bubble/particle aggregate

P_{stab} - probability of stability of a bubble/particle aggregate

P_{tpc} - probability of the formation of a three-phase contact

R_B - bubble radius

Re_B - bubble Reynolds number

Re_B^* - $\frac{1}{15} Re_B^{0.72}$

Re_p - particle Reynolds number

R_p - particle radius

$\bar{U}_B$ - relative velocity between a bubble and the fluid

$\bar{U}_p$ - relative velocity between a particle and the fluid

Z - collision frequency divided by the number of bubbles available to capture particles at time $t > 0$.

Z' - detachment frequency of particles from bubbles

d_p - particle diameter

erf (x) - error function

f - fluid flow friction factor

g - acceleration due to gravity

$g(r)$ - $\left(1 - \frac{3R_B}{4r} - \frac{R_B^3}{4r^3}\right) + Re_B^* \left(\frac{R_b}{r} + \frac{R_B^3}{r^3} - \frac{2R_b^4}{r^4}\right)$

h_0 - initial thickness of the film separating a bubble and a particle

h_{crit} - film thickness at which the film ruptures spontaneously

$k(r)$ - $\left\{\left(1 - \frac{3R_B}{2r} + \frac{R_B^3}{2r^3}\right) + 2Re_B^* \left(\frac{R_B^4}{r^4} - \frac{R_B^3}{r^3} - \frac{R_B^2}{r^2} + \frac{R_B}{r}\right)\right\}$

k_1 - forward (attachment) rate parameter

k_2 - reverse (detachment) rate parameter

$\bar{k}_1$ - $ZP_cP_{asl}P_{tpc}P_{stab}$

n_B - constant (total) bubble concentration

n_B^A - concentration of bubbles available to capture particles

n_B^a - concentration of bubbles with attached particles

n_B^f - free bubble concentration

$n_B^{a,j}$ - concentration of bubbles with j particles attached, $0 \leq j \leq K$.

n_p - constant particle concentration

n_p^f - concentration of free particles

n_{po} - initial concentration of particles ($\equiv n_{po}^f$)

n_{po}^f- initial concentration of free particles

r - radial distance from the center of a bubble

v_B - bubble rise velocity

v_p - particle velocity

v_{ps} - particle settling velocity

$\Lambda(t)$- average number of particles, at time t, which are attached to a bubble in the exit stream

$\bar{\Lambda}$ - time averaged Λ, i.e., $\frac{1}{T}\int_0^T \Lambda(t)dt$

$\sum$ - summation symbol

α - system parameter mediating the stability of bubble/particle aggregates

ϵ - (Kolmogorov) turbulent energy density

γ - n_p^f/n_{po}^f

$\tilde{\lambda}$ - dimensionless friction factor

μ_l - fluid viscosity

ν_l - kinematic viscosity

ρ_B - bubble (gas) density

ρ_l - fluid density

ρ_p - particle density

σ - surface tension

$\bar{\sigma}$ - standard deviation of a normally distributed random variable

θ - contact angle

Experiment number	Feed Flow Rate (GPM)	Feed Consistency (%)
1	4040	1.24
2	3640	1.24
3	3640	1.11
4	4030	1.37
5	4440	1.24

Table 1: Factors varied during the mill trial.

Experiment #1	Cycle 1 (dynes/cm)	Cycle 2 (dynes/cm)	Ave. Surface Tension (dynes/cm)
Discharge Cells			
1	49.32	49.11	49.22
2	49.43	49.30	49.37
3	46.35	46.87	46.61
4	50.60	50.57	50.59
5	49.21	49.11	49.16
6	46.74	47.04	46.89
Overflow Cells			
1	42.02	42.31	42.17
2	41.36	41.71	41.54
3	44.21	43.58	43.90
4	43.98	43.48	43.73
5	43.12	43.00	43.06
6	44.50	44.04	44.27
Mixcell Discharge	49.73	50.28	50.01
Feedflow	50.77	50.51	50.64
Accepts from 2nd Secondary Cell	44.93	45.15	45.04
Rejects 1-6 from Primary Cell	45.93	45.58	45.76
Flotation Accepts	48.57	48.63	48.60

Table 2: Surface Tension measurements on filtrates from pulp samples

Experiment #2	Cycle 1 (dynes/cm)	Cycle 2 (dynes/cm)	Ave. Surface Tension (dynes/cm)
Discharge Cells			
1	49.26	49.20	49.23
2	47.97	47.68	47.83
3	47.09	46.80	46.95
5	48.72	48.66	48.69
6	50.71	50.50	50.61
Overflow Cells			
1	41.25	40.85	41.05
3	44.08	44.08	44.08
6	44.27	43.85	44.06
Feed Pump	46.39	46.15	46.27
Primary Accepts from Cell 7	46.41	47.71	47.06
Primary Rejects	45.00	44.44	44.72
Discharge Cell 2	48.66	48.13	48.40

Table 3: Surface Tension measurements on filtrates from pulp samples.

Experiment #3	Cycle 1 (dynes/cm)	Cycle 2 (dynes/cm)	Ave. Surface Tension (dynes/cm)
Discharge Cells			
1	49.60	49.14	49.37
2	46.22	46.39	46.31
3	48.66	48.53	48.60
5	48.90	48.10	48.50
6	49.83	49.40	49.62
Overflow Cells			
1	43.66	43.22	43.44
3	44.81	44.31	44.56
6	42.55	42.00	42.28
Mixcell Discharge	46.89	46.75	46.82
Feedflow	51.02	50.51	50.77
Primary Accepts from Cell 7	49.66	49.94	49.80
Primary Rejects	45.53	45.02	45.28

Table 4: Surface Tension measurements on filtrates from pulp samples.

Experiment #4	Cycle 1 (dynes/cm)	Cycle 2 (dynes/cm)	Ave. Surface Tension (dynes/cm)
Discharge Cells			
1	49.17	48.83	49.00
2	50.43	50.14	50.29
3	48.87	48.49	48.68
5	45.46	45.90	45.68
6	46.90	47.14	47.02
Overflow Cells			
1	44.20	44.45	44.33
3	45.67	45.67	45.67
6	43.72	43.34	43.53
Mixcell Discharge	50.80	50.08	50.44
Feedflow	46.41	46.84	46.63
Primary Accepts from Cell 7	49.00	49.12	49.06
Primary Rejects	40.42	41.27	40.85

Table 5: Surface Tension measurements on filtrates from pulp samples.

Experiment #5	Cycle 1 (dynes/cm)	Cycle 2 (dynes/cm)	Ave. Surface Tension (dynes/cm)
Discharge Cells			
1	46.46	46.47	46.47
2	47.85	47.66	47.76
3	48.72	48.70	48.71
5	49.36	49.55	49.46
6	46.64	46.64	46.64
Overflow Cells			
1	43.63	43.18	43.41
3	42.14	41.98	42.06
6	41.16	41.03	41.10
Mixcell Discharge	49.62	49.21	49.42
Feedflow	47.43	47.35	47.39
Primary Accepts from Cell 7	49.91	49.67	49.79
Primary Rejects	45.79	45.25	45.52
Primary Rejects	42.86	43.17	43.02

Table 6: Surface Tension measurements on filtrates from pulp samples.

Experiment	Feed-Eric values	Accepts-Eric values
1	924.3	221.8
2	971.6	238.1
3	929.6	199.4
4	956.7	248.25
5	839.8	233.8

Table 7: ERIC measurements on handsheets.

Experiment	Particle Size(μm)	# Particles in Feed	# Particles in Accepts	Experimental Efficiency
1	8-20	11897	1316	88.93
1	24-52	1932	184	90.47
1	56-224	94	30	68.1
2	8-20	10942	1567	85.60
2	24-52	1524	220	85.60
2	56-224	69	34	50.72
3	8-20	11543	1164	89.91
3	24-52	1643	235	85.60
3	56-224	89	30	66.29
4	8-20	13323	1283	90.37
4	24-52	1771	252	85.77
4	56-224	105	32	69.52
5	8-20	11348	1429	87.40
5	24-52	1440	263	81.70
5	56-224	119	42	64.70

Table 8: Dirt count measurement on handsheets.

Parameter	Initial Value
	0.2/0.7
Bubble Radius	750 microns
# of Bubbles	3.96E+08
Particle Radius	10 microns
# of Particles	3.00E+07
Turbulent Energy Density	50.26
Gas hold up	0.10
Surface Tension	50 dynes/cm
Contact Angle	60 degrees
Viscosity	$1mm^2/sec$
Bubble density	$0.001\ kg/m^3$
Fluid density	$1000\ kg/m^3$
Particle density	$1200\ kg/m^3$

Table 9: Parameter values used in calculating predicted long time efficiency.

Particle Size	Experiment number	Model Efficiency	Experimental Efficiency
10 microns	1	89.36	88.94
	3	89.54	89.92
	4	89.03	90.37
50 microns	1	85.98	90.48
	3	86.04	85.70
	4	85.98	85.77

Table 10: Comparison of experimental and predicted efficiency.

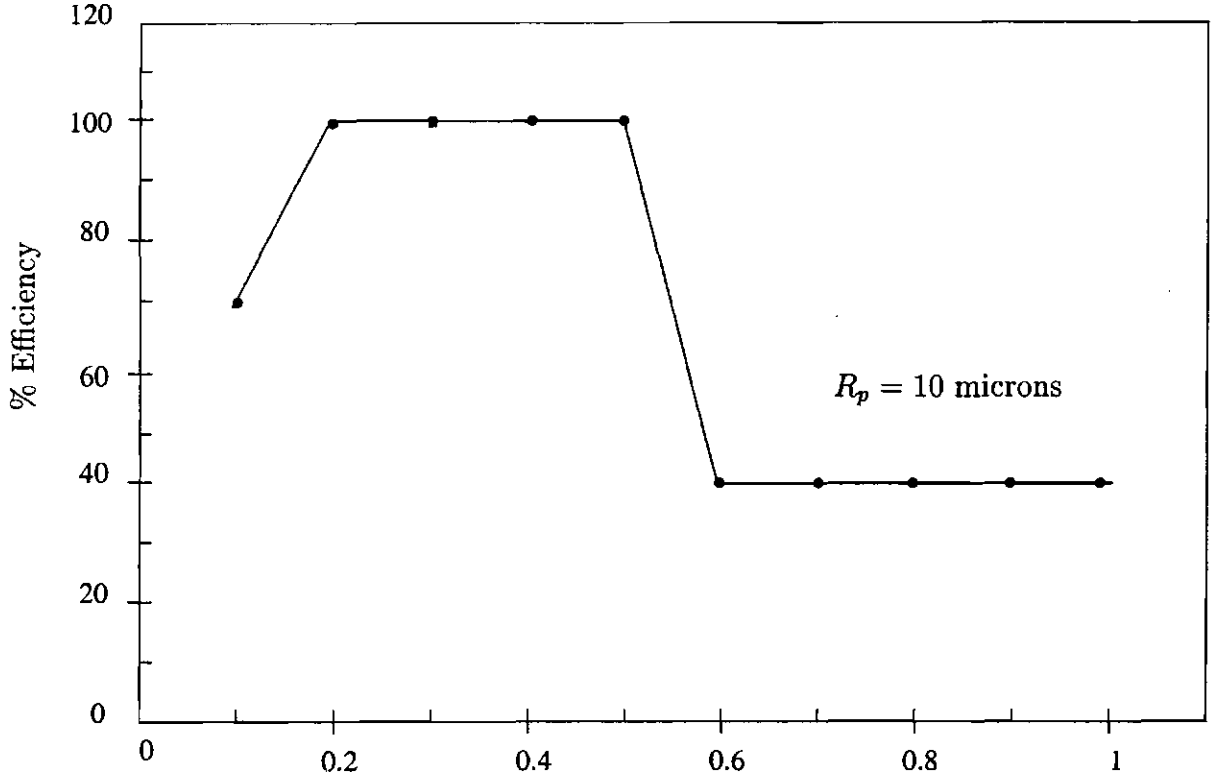

Figure 1: Effect of parameter α on the predicted long time efficiency ($R_p = 10\mu$m)

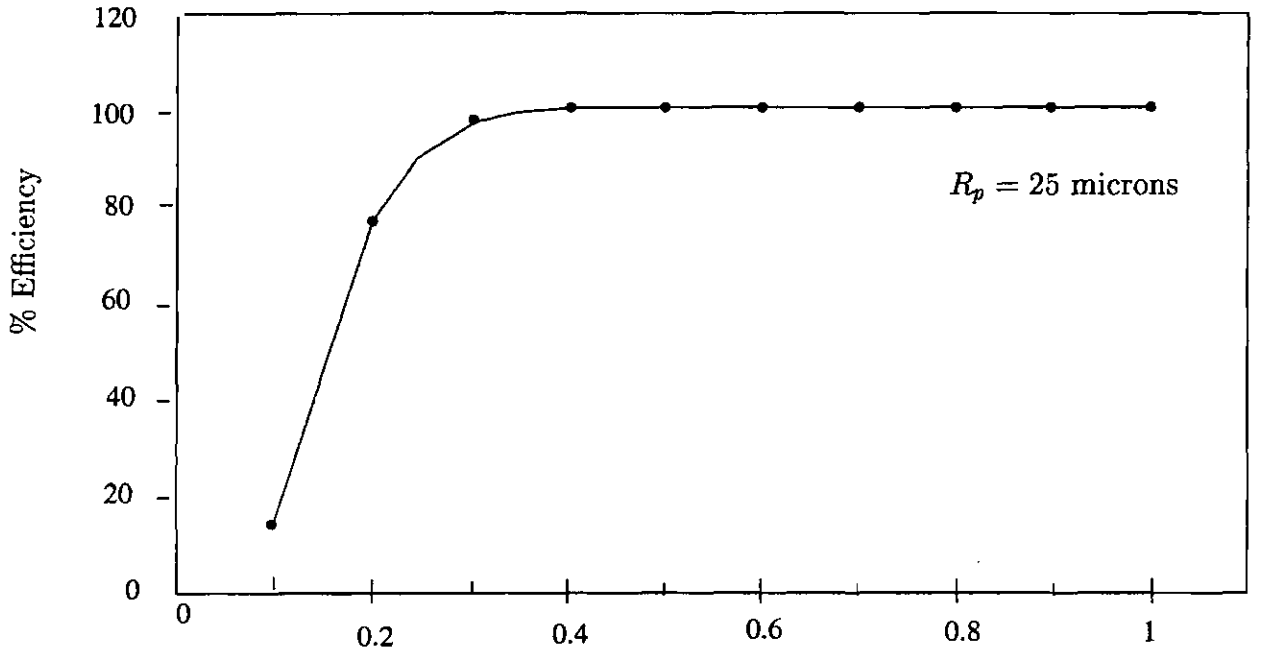

Figure 2: Effect of parameter α on the predicted long time efficiency ($R_p = 25\mu$m)

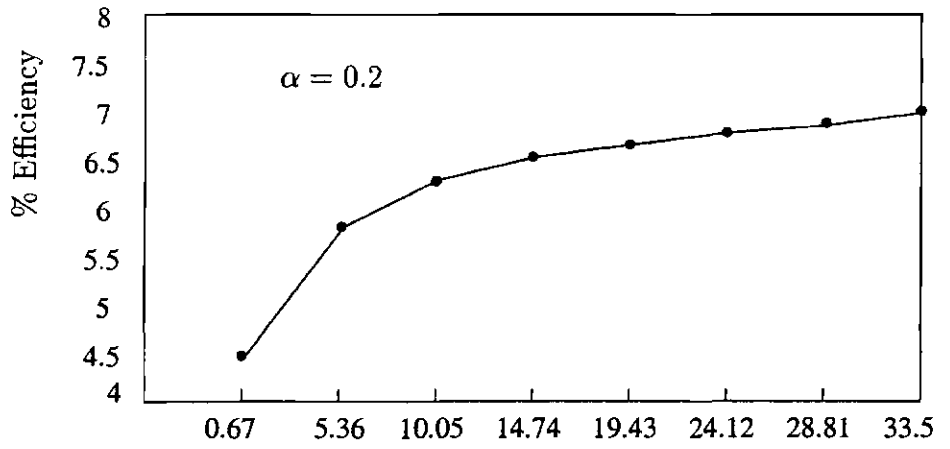

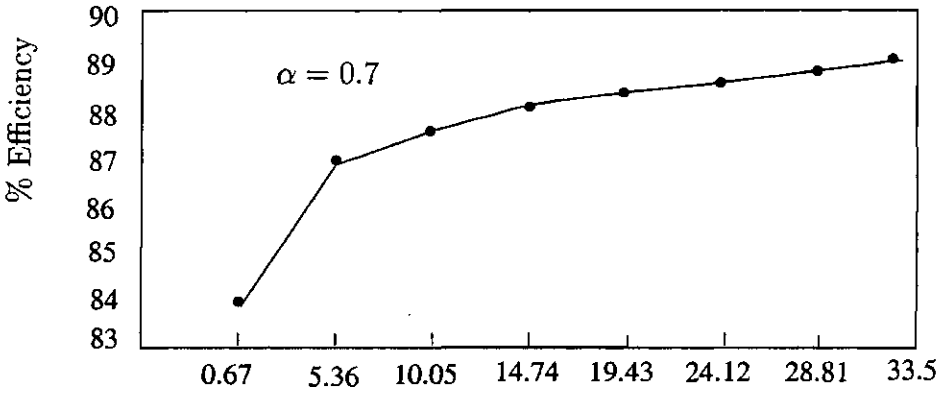

Figure 3: Turbulent energy density versus percent efficiency for α equal to 0.2 and 0.7 respectively.

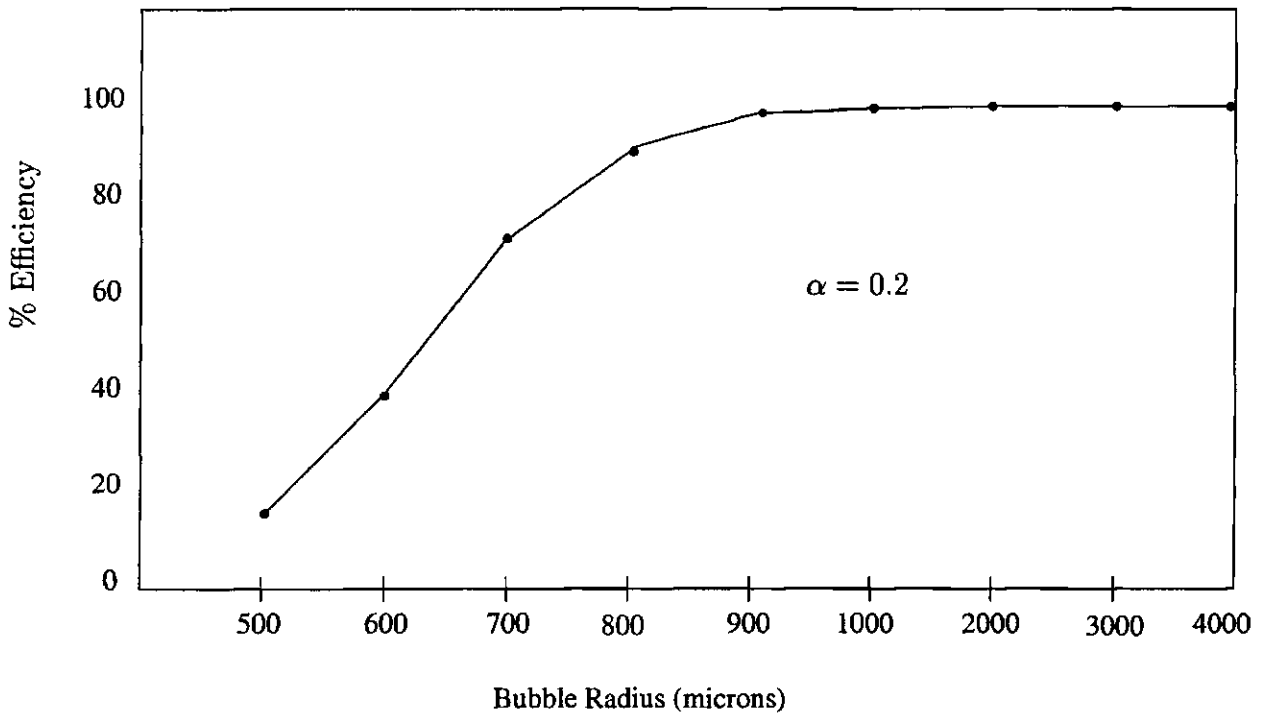

Figure 4: Dependence of predicted long time efficiency on bubble radius (R_B).

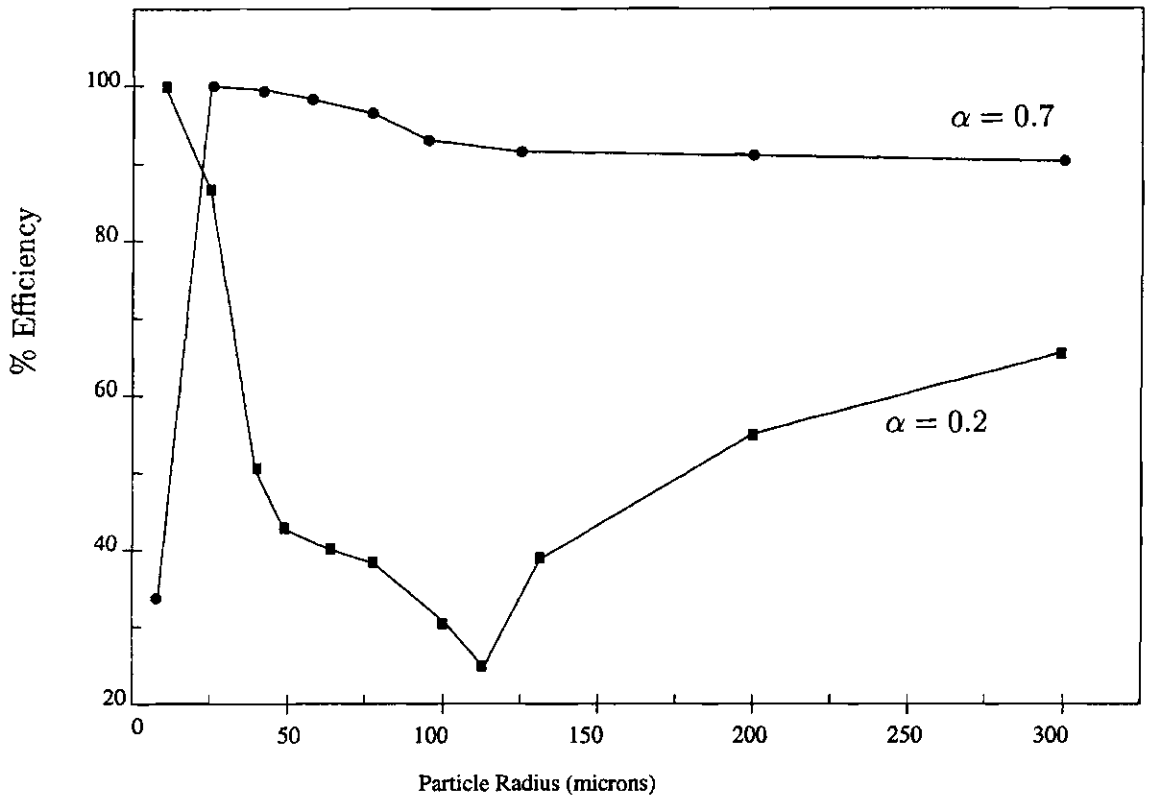

Figure 5: Dependence of predicted long time efficiency on particle radius (R_p).

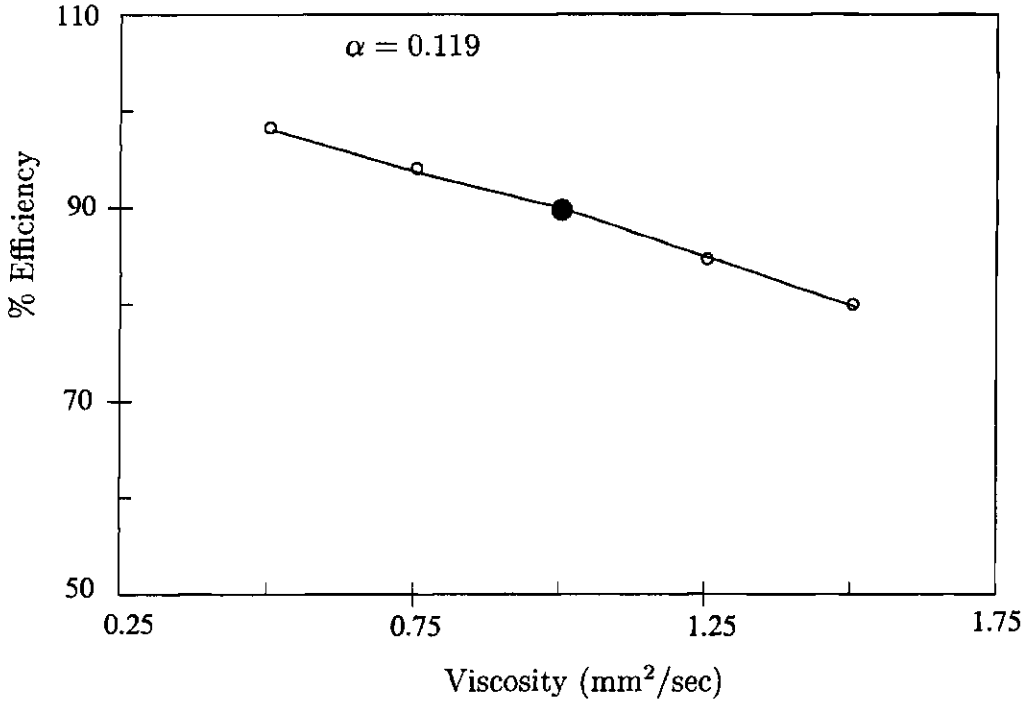

Figure 6: Effect of viscosity on predicted long time efficiency.

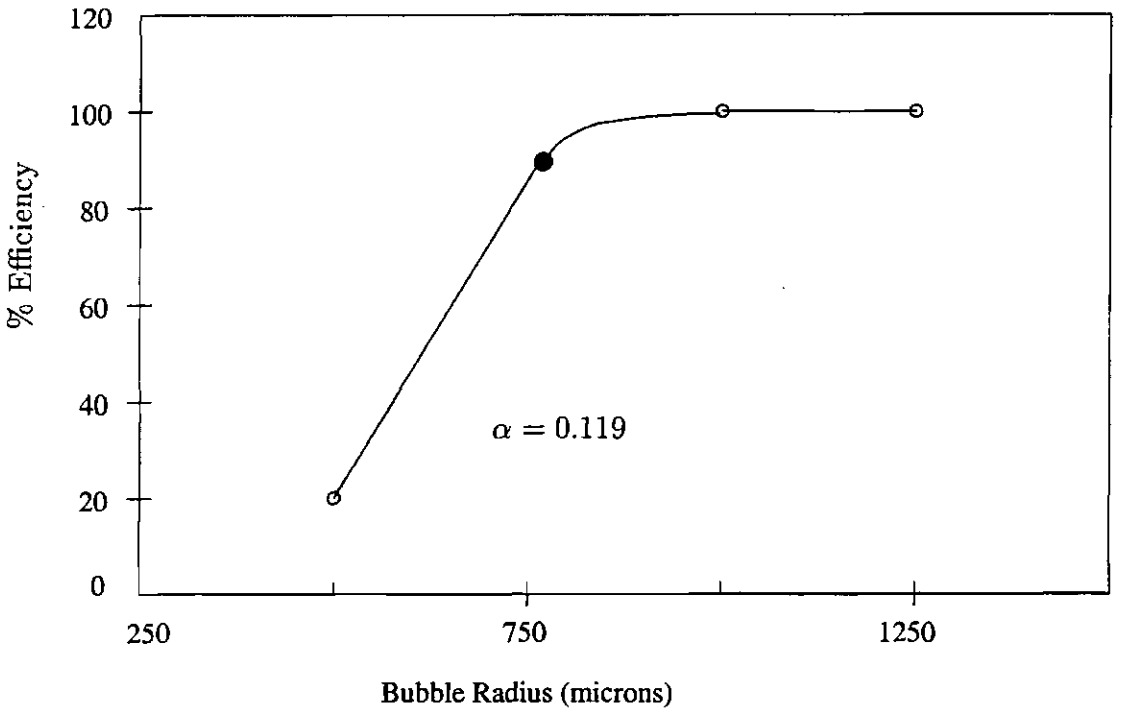

Figure 7: Effect of bubble radius on predicted long time efficiency for $\alpha = 0.119$